Influence of angular momentum and Coulomb interaction of colliding nuclei on their multifragmentation

A. Ergun, H. Imal, N. Buyukcizmeci,* and R. Ogul
Department of Physics, University of Selçuk, 42079 Konya, Turkey

A. S. Botvina
Institute for Nuclear Research, Russian Academy of Sciences, 117312 Moscow, Russia, and Frankfurt Institute for Advanced Studies, J. W. Goethe University, D-60438 Frankfurt am Main, Germany

(Received 12 August 2014; revised manuscript received 1 May 2015; published 9 July 2015)

Theoretical calculations are performed to investigate the angular momentum and Coulomb effects on fragmentation and multifragmentation in peripheral heavy-ion collisions at Fermi energies. Inhomogeneous distributions of hot fragments in the freeze-out volume are taken into account by microcanonical Markov chain calculations within the statistical multifragmentation model. Including an angular momentum and a long-range Coulomb interaction between projectile and target residues leads to new features in the statistical fragmentation picture. In this case, one can obtain specific correlations of the sizes of emitted fragments with their velocities and an emission in the reaction plane. In addition, one may see a significant influence of these effects on isotope production both in the midrapidity and in the kinematic regions of the projectile/target. The relation of this approach to the simulations of such collisions with dynamical models is also discussed.

DOI: 10.1103/PhysRevC.92.014610 PACS number(s): 25.70.Pq

I. INTRODUCTION

It has long been commonly accepted that in central heavy-ion collisions at Fermi energies (20–50 MeV per nucleon) relatively high excitation energies of nuclear matter, with temperatures up to $T \approx 5$–8 MeV, can be reached [1]. Therefore, they become a suitable tool for study of the equation of state of hot nuclear matter and nuclear liquid-gas phase transitions at subnuclear densities. As discussed previously [2], with the help of multifragmentation one can study the properties of hot fragments in the vicinity of other nuclear species. The angular momentum effect is usually disregarded in this case, since the impact parameters are small. During peripheral heavy-ion collisions at the same energies, a considerable amount of angular momentum can be transferred from the interaction region to the excited projectile and target residual nuclei, and this can lead to significant changes in their multifragmentation [3–5]. Additional long-range forces caused by the complicated Coulomb interaction between the target and projectile-like sources are involved essentially in the process [5,6]: Multifragmentation in the presence of an external Coulomb field offers the possibility to study, experimentally, the effects of this long-range force, which are very important for disintegration of matter [4]. This is also necessary for construction of a reliable equation of state of nuclear matter at subnuclear densities. Another motivation for these studies is that similar conditions for nuclear matter occur during the collapse and explosion of massive stars and in the crust of neutron stars [7,8], where the Coulomb interactions of the dense electron environment change the fragmentation picture. It is generally assumed that the statistical equilibrium regarding fragment composition at subnuclear densities should be established in these astrophysical cases. Therefore, analysis of the observables obtained in laboratory experiments with statistical models is a proper way to get knowledge on stellar matter. Previous studies of the isospin composition of the produced fragments were found to be especially important for determining the strength of the symmetry energy during fragment formation in hot and diluted environments [2,9–11].

In the analysis of ALADIN data, charge and isotope yields, fragment multiplicities and temperatures, and correlations of various fragment properties were successfully described by the statistical ensemble approach [11–16] within the statistical multifragmentation model (SMM) [17]. This was also achieved in the analysis of the experimental data of Liu *et al.* [18] obtained at the MSU laboratory at 50 MeV/nucleon [19–21] and in the analysis of TAMU data [22,23]. In these studies, the symmetry energy of fragments was one of the main model parameters governing the mean N/Z values, the isoscaling parameters, and the isotopic composition of the fragments. For interpretation of ALADIN and MSU experiments, which can be explained by formation and decay of single thermalized sources, we considered the averaged Coulomb interaction of fragments (Wigner-Seitz approximation), since the direct positioning of fragments in the freeze-out volume has a minor influence on their charge and isotope distributions. This is well justified for relativistic peripheral collisions and for central collisions of heavy nuclei around the Fermi energy. However, important information on multifragmentation and properties of fragments can be extracted in peripheral collisions at Fermi energies as well. The new fragment partitions can be obtained by including the Coulomb effects caused by the proximity of colliding target and projectile nuclei, as well as those caused by the large angular momentum transfer to the multifragmentating sources. For example, a long-range Coulomb interaction of the target- and projectile-like sources changes the fragmentation

*nihal@selcuk.edu.tr

pattern and leads to a predominant emission of light and intermediate-mass fragments (IMFs; with charge numbers $Z = 3$–20) towards the midrapidity, i.e., in the direction of another source [6,24]. A few such experiments have been analyzed with statistical models [23,25]. However, there were no systematic theoretical investigations of the Coulomb and angular momentum effects on the multifragmentation picture in these reactions, especially on the isotope yields, which are crucial for astrophysical applications. As suggested in Refs. [5] and [6], the angular momentum may lead to more neutron-rich IMF production and to anisotropic emission with respect to the projectile and target sources.

In this paper, we theoretically investigate the influence of angular momentum and Coulomb interactions on the charge yields, the neutron-to-proton ratios, and the velocity distributions of hot particles for peripheral $^{84}\mathrm{Kr} + {}^{84}\mathrm{Kr}$ collisions at 35 MeV per nucleon. We believe that this is a quite typical reaction, and our selection is partly motivated by recent FAZIA experiments [26]. For simulation of the reactions, we consider the breakup of a single-source ^{84}Kr in the proximity of a secondary-source ^{84}Kr, as a symmetric system in terms of isospin contents. Calculations are carried out within the Markov chain version of the SMM, which is designed for microcanonical simulation of the decay modes of nuclear sources [5,24]. This method is based on producing the Markov chain of partitions which characterize the whole statistical ensemble. In this method the individual fragment partitions and coordinate positions of fragments in the freeze-out volume are generated. They are selected by the Metropolis algorithm and we can take into account the influences of the angular momentum and Coulomb interactions for each spatial configuration of primary fragments in the freeze-out volume, similarly to Refs. [3,4].

Usually, the conception of statistical sources under multifragmentation is quite effective for description of relativistic nucleus-nucleus collisions [11,15–17]. We believe that new effects which may be expected within the statistical picture in low-energy reactions can be important at high energies too. In particular, this can help to clarify possible deviations from poor statistical disintegration that may exist in the fragment sources produced in relativistic collisions.

II. STATISTICAL APPROACH TO MULTIFRAGMENTATION

It is assumed in the microcanonical SMM that a statistical equilibrium is reached in the low-density freeze-out region. The breakup channels are composed of nucleons and nuclear fragments, and the laws of conservation of energy E_x, momentum, angular momentum, mass number A, and charge number Z are considered. Besides the breakup channels, the compound-nucleus channels are also included, and competition among all channels is permitted. In this way, the SMM covers the conventional evaporation and fission processes occurring at low excitation energies as well as the transition region between the low- and the high-energy de-excitation regimes. In the thermodynamic limit, SMM is consistent with liquid-gas phase transitions when the liquid phase is represented by infinite nuclear clusters [27], which allow connections for the astrophysical cases [28]. We calculate the statistical weights of all breakup channels partitioning the system into various species. The decay channels are generated by the Monte Carlo method according to their statistical weights. In the Markov chain SMM [5,24] we also use ingredients taken from the standard SMM version developed in Refs. [17,29,30], which was successfully used for comparison with various experimental data: Light fragments with mass number $A \leqslant 4$ and charge number $Z \leqslant 2$ are considered elementary particles with the corresponding spins (nuclear gas) that have translational degrees of freedom. Fragments with mass number $A > 4$ are treated as heated nuclear liquid drops. In this way one can study nuclear liquid-gas coexistence in the freeze-out volume. Free energies $F_{A,Z}$ of each fragment are parameterized as the sum of the bulk, surface, Coulomb, and symmetry energy contributions:

$$F_{A,Z} = F^B_{A,Z} + F^S_{A,Z} + E^C_{A,Z} + E^{\mathrm{sym}}_{A,Z}. \tag{1}$$

The bulk contribution is given by $F^B_{A,Z} = (-W_0 - T^2/\varepsilon_0)A$, where T is the temperature (which is found for each channel using the energy conservation), the parameter ε_0 is related to the level density, and $W_0 = 16$ MeV is the binding energy of infinite nuclear matter. The contribution of the surface energy is $F^S_{A,Z} = B_0 A^{2/3}[(T_c^2 - T^2)/(T_c^2 + T^2)]^{5/4}$, where $B_0 = 18$ MeV is the surface energy term and $T_c = 18$ MeV the critical temperature of the infinite nuclear matter. In the standard SMM version the Coulomb energy contribution is $E^C_{A,Z} = cZ^2/A^{1/3}$, where c denotes the Coulomb parameter obtained in the Wigner-Seitz approximation, $c = (3/5)(e^2/r_0)(1 - (\rho/\rho_0)^{1/3})$, with the charge unit e, $r_0 = 1.17$ fm, and ρ_0 is the normal nuclear matter density (0.15 fm^{-3}). However, within this Markov-chain SMM we directly calculate the Coulomb interaction of nonoverlapping fragments in the freeze-out by taking into account their real coordinate positions. The symmetry term is $E^{\mathrm{sym}}_{A,Z} = \gamma(A - 2Z)^2/A$, where $\gamma = 25$ eV is the symmetry energy parameter. All the parameters given above are taken from the Bethe-Weizsaecker formula and correspond to the assumption of isolated fragments of a normal density unless their modifications in the hot and dense freeze-out configuration follow the analysis of experimental data. For the freeze-out density, one-third of the normal nuclear matter density is assumed in many successful studies and consistent with independent experimental determination in sources formed in peripheral nuclear collisions [31,32]. To be more general, in this work we use $\rho = \rho_0/2$ and $\rho = \rho_0/6$ densities for better evaluation of Coulomb and angular momentum effects. The various positioning of particles and volume parameters is also useful for understanding the origin of the kinetic energies of fragments observed in experimental data. In the case of the high density ($\rho = \rho_0/2$) we assume a deformation of fragments in the freeze-out volume by effectively reducing distances between the fragments for calculation of their Coulomb interaction by a factor of 0.7. This can be partly justified by the nonspherical shape of these fragments since they are excited. Usually, we generate about 5×10^5 Monte Carlo events to provide sufficient statistics.

III. EFFECTS OF ANGULAR MOMENTUM AND COULOMB INTERACTION OF PROJECTILE- AND TARGET-LIKE SOURCES

As mentioned we investigate only the statistical decay of excited sources produced in peripheral collisions. Many dynamical features, such as the neck-like emission of fragments and isospin diffusion between the sources during collisions are beyond the scope of this work. In some cases the dynamical effects could be taken as input for the statistical stage, for example, by adjusting N/Z ratios of the sources, Coulomb interactions during the disintegration of the sources, and their angular momentum. For peripheral nucleus-nucleus collisions at 35 MeV/nucleon the corresponding relative velocity between projectile and target is about 80 mm/ns. As discussed within the standard reaction picture, during the initial dynamical stage of such a collision, projectile nucleons interact with target nucleons and some energetic products of this interaction can leave the nuclei as pre-equilibrium particles. The kinetic energy of colliding nuclei can also be converted into the excitation energy of projectile and target residues. Therefore, the relative velocity between the residues decreases as well. These excited target- and projectile-like sources decay afterwards.

It is known that nuclear multifragmentation is a fast process, within a characteristic time around 100 fm/c. Therefore, projectile- and target-like sources will not be far from each other before disintegration. The idea is that at these short distances the long-range Coulomb field of one of the sources influences the breakup of the other one. In this case we are dealing with multifragmentation in a double-nuclear system, which is a new physical situation with respect to the standard multifragmentation of a single isolated source.

According to our estimates from the energy conservation, their relative velocity should decrease to ∼50 mm/ns, at an excitation energy around 5 MeV/nucleon transferred to the residues. In this case, they will be separated by ≈15 fm in a time of 100 fm/c. The decay of the two excited sources in such a double system is determined by the short-range nuclear forces. However, the presence of an external Coulomb field (for each source) can affect the composition of the produced fragments and their relative positions. In particular, an additional Coulomb barrier will prevent disintegration of the sources into many small pieces. In this work we do not include the possible deformation of the sources after the dynamical stage in order to separate the Coulomb effects. It should also be noted that during the evolution of a double system we must take into account its total center-of-mass conservation without an additional constraint in the freeze-out volumes of disintegrating sources. On the other hand, we include the angular momenta (rotation) of the separate sources, which can be transferred after the collision. It will also influence the positions and sizes of the fragments at freeze-out [3,5,6]. In the following we probe the upper estimate of the angular momentum $80\hbar$ in order to see its effect clearly.

We demonstrate the results for multifragmentation of the projectile-like source (we call it the first source) by assuming the Coulomb field coming from the center of the target source (the second source). The first source is assumed to fly along the Y axis, and the second one is in the opposite direction (related to the center of mass of the double system). This separation axis may slightly deviate from the initial beam axis. The location of the second source is taken as $R_Y = -10.6$ fm and $R_Z = 10.6$ fm with respect to the first source, for the 15 fm of separation. The peripheral collision is assumed to take place in the Y-Z plane, therefore, the coordinates on the Z axis are determined by the sizes of colliding nuclei, as well as by their possible repulsion after the collision. The X axis is assumed to be an angular momentum axis. We suggest that this relative space configuration of the sources is quite general and suitable for investigating Coulomb and angular momentum effects.

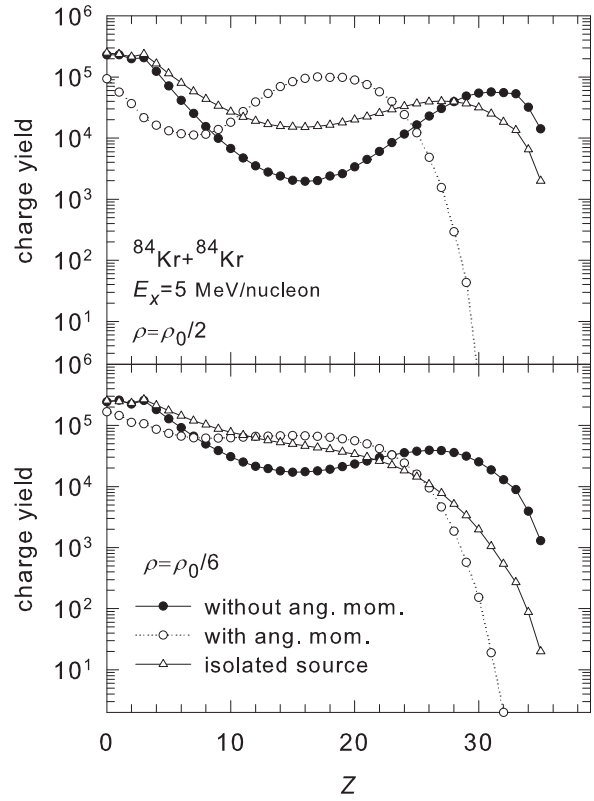

FIG. 1. Total charge yield of primary hot fragments, in cases without (filled circles) and with (open circles; $L = 80\hbar$) angular momentum, after multifragmentation of the projectile ^{84}Kr source at excitation energy $E_x = 5$ MeV/nucleon. This source is assumed to be formed in the peripheral ^{84}Kr + ^{84}Kr collision at 35 MeV/nucleon, and its disintegration is affected by the Coulomb field of the target source. Results at freeze-out densities $\rho = \rho_0/2$ (top) and $\rho = \rho_0/6$ (bottom). For comparison, the results of multifragmentation of a single isolated ^{84}Kr source, at the same excitation energy but without the external Coulomb field and without angular momentum, are also shown.

The pre-equilibrium emission of a few nucleons during the dynamical stage may decrease the excitation energy and relative velocity of the residues. However, this can be accounted for in the statistical approach by changing the corresponding input and by using the ensemble of the sources (see, e.g., [11]) with adequate parameters. On the other hand, as shown in many theoretical and experimental works (see, e.g., [12,17,33]), the relative yields of IMF do not depend much

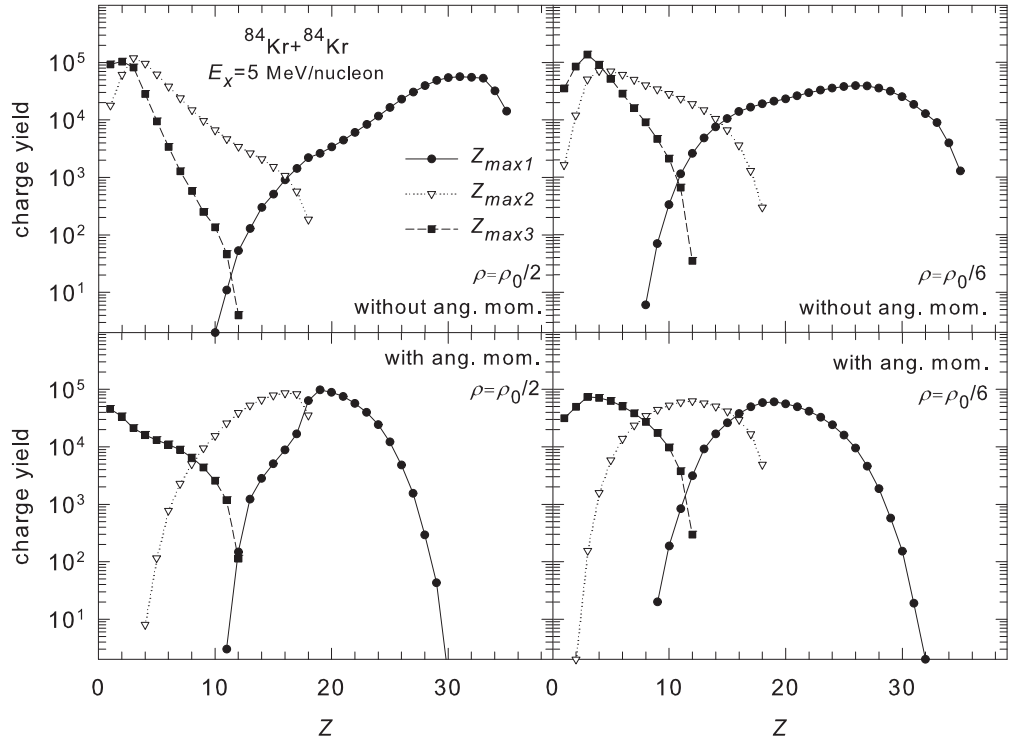

FIG. 2. Charge yield of the first, second, and third largest hot fragments (Z_{max1}, Z_{max2}, and Z_{max3}) after multifragmentation of the ^{84}Kr source (as in Fig. 1). Results without angular momentum (top panels) and with angular momentum ($L = 80\hbar$) (bottom panels).

on the size of the sources in the multifragmentation regime (a scaling effect). Therefore, for our purposes it is sufficient to consider sources of the same size and isospin content as the colliding nuclei (^{84}Kr).

A. Charge distributions

The purpose of our analysis is to understand the new characteristics of fragment distributions, which are necessary for interpretation of many experiments on heavy-ion collisions at Fermi energies. We consider the angular momentum and Coulomb field influences on the charge and isospin contents of produced fragments and compare them with the standard calculations without these effects. It is expected that the correlations of the sizes and $\langle N\rangle/Z$ of hot fragments with their velocities will be important. For this purpose, after the breakup of the sources we calculate the Coulomb propagation of produced hot fragments by taking into account the Coulomb interactions of particles and their velocities at the breakup time. In this paper, in order to clarify the modification of the multifragmentation picture caused by the new effects, we do not apply the secondary de-excitation of the hot fragments, which, however, can lead to important consequences, especially for the isospin composition of final fragments.

In the beginning, we consider the effects corresponding to the short distance (15 fm) between the sources. In Fig. 1, we show the total charge yields of hot fragments in the cases with and without angular momentum conservation. It is shown that the charge distributions are very sensitive to the freeze-out densities. The angular momentum favors emission of large nearly symmetric fragments (like nuclear fission) since the system at freeze-out needs to have a large moment of inertia in order to minimize the rotational energy and maximize the entropy. It is in competition with the second source influence through the Coulomb interaction, which prevents the emission of an IMF with a large charge number. The latter can be seen clearly in comparison with the case of fragmentation of a standard single isolated source.

For more details, we show in Fig. 2 the yield distributions of the first, second, and third largest fragments versus their charge numbers Z_{max1}, Z_{max2}, and Z_{max3}, respectively. These observables are used to obtain complementary information on the fragmentation pattern. Top panels include the long-range Coulomb contribution from the second source only, and bottom panels include, in addition, the angular momentum effects. It is obvious that the distributions of Z_{max1}, Z_{max2}, and Z_{max3} are ordered according to their size. In the case where the angular momentum is included (bottom panels), the average value of Z_{max1} decreases, while Z_{max2} and Z_{max2} show an increasing trend. A low freeze-out density ($\rho = \rho_0/6$) leads to the smoother and broader distributions (sometimes Gaussian-like) caused by the less restricted population of the larger coordinate phase space.

B. $\langle N\rangle/Z$ and velocity distributions

The initial value of the neutron-to-proton ratio (N/Z) of the source ^{84}Kr is 1.33. In Fig. 3, we see that the angular momentum leads to increasing N/Z values of IMFs in the case of strongly asymmetric decay. This is also caused by the increasing moment of inertia of the system, which favors a bigger phase space of the reaction [5]. It is a very instructive trend which could be responsible for many isospin observables.

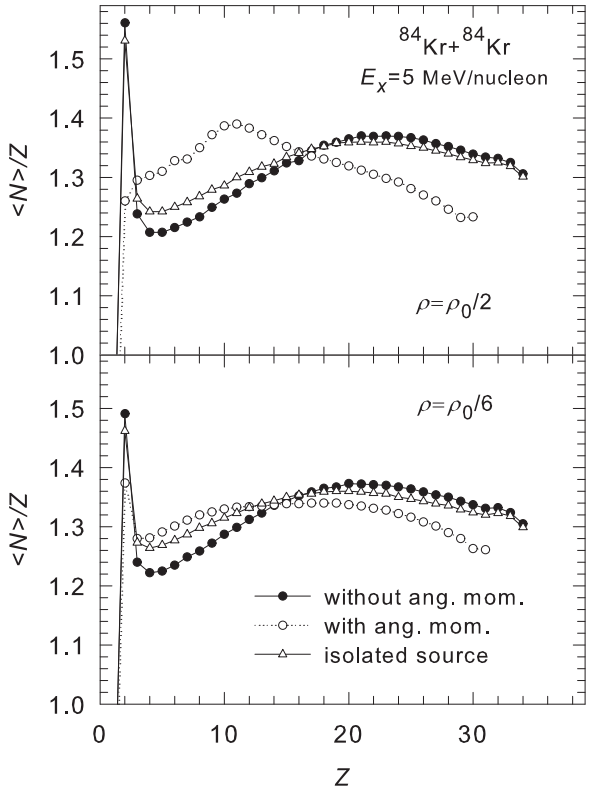

FIG. 3. Mean neutron-to-proton ratios $\langle N\rangle/Z$ of hot primary fragments produced at the freeze-out density $\rho = \rho_0/2$ (top) and $\rho = \rho_0/6$ (bottom). Other notation is as in Fig. 1.

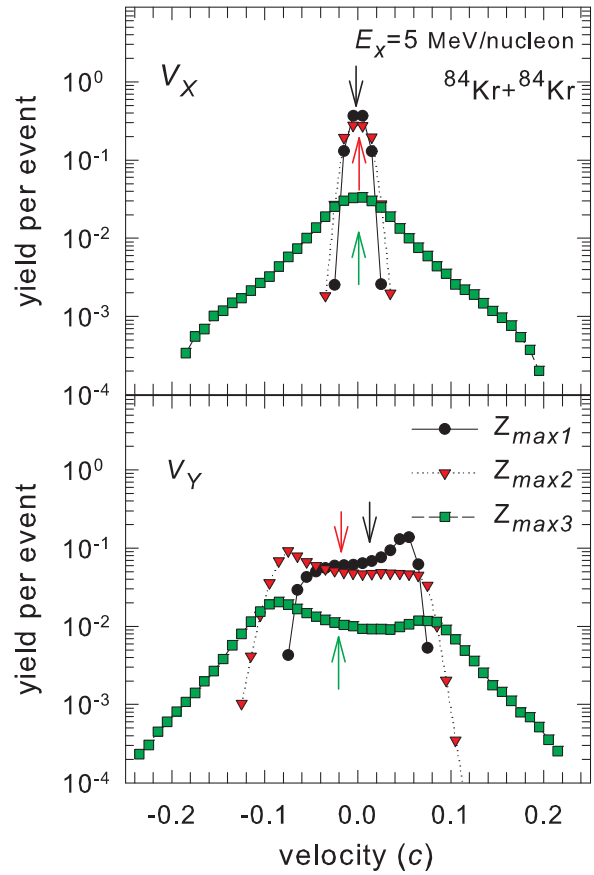

FIG. 4. (Color online) V_X and V_Y velocity distributions of the first, second, and third largest fragments in multifragmentation of ^{84}Kr with angular momentum $L = 80\hbar$ and at freeze-out density $\rho = \rho_0/2$, in the source frame.

In Fig. 4, we present the yields per event as a function of the velocities V_X and V_Y for the fragments having the first, second, and third largest charge numbers, in the first source frame. The V_X velocity distributions in the direction of the angular momentum are shown in the top panel. The first and second fragments are nearly peaked around 0, and this means that they are emitted mostly in the V_Y-V_Z plane. This is very different from the case of isotropic statistical emission taking place without angular momentum, which is sometimes simplistic assumed to be the only possibility for the statistical breakup. In our case all these fragments fly predominantly in the plane of rotation, even though the smallest fragments can deviate from this plane. Another important effect is shown in the bottom panel in Fig. 4. We remember that the velocity V_Y determines the separation axis (close to the beam axis), where the sources move in opposite directions. One can see that there is an order in the emission of fragments of different sizes, such that the largest fragments have the highest velocity V_Y, which is higher than those of the second and third ones. The arrows refer to the average values of the velocity distributions. The maximum fragments fly predominantly in the forward direction as $V_Y > 0$, while the second and third ones fly in the backward direction as $V_Y < 0$ (i.e., to the direction of the target source), and in this way they may simulate the so-called "midrapidity emission." This is the consequence of the fragment coordinate positions occupied predominantly in the freeze-out, and this is caused mainly by the Coulomb repulsion of the second source. This effect is consistent with previous experimental observations [34]. Its dynamical interpretation may also be possible, however, the contribution of the Coulomb interaction has not been separated or investigated up to now with dynamical models.

For detailed examination of the characteristics of produced particles, we show in Fig. 5 the relative yields (normalized per total number of generated events) of the hot primary fragments with $Z = 3$, 6, 9, 12, 15, and 18 versus their velocities along the separation axis V_Y. As in Fig. 4, these velocities are calculated with respect to the projectile source, so that $V_Y < 0$ means an emission towards the midrapidity. The figure demonstrates clearly the predominantly "backwards" emission for the light IMF changing to a " uniform-like" emission for larger fragments. It is very important to investigate the isospin content of these fragments. Their $\langle N\rangle/Z$ ratio versus V_Y is demonstrated in Fig. 6. One can see in this figure that including the angular momentum can lead to increasing $\langle N\rangle/Z$ ratios for small fragments. The external Coulomb field leads to the emission of neutron-rich fragments towards the midrapidity. This trend is clearly seen for $Z = 3$, $Z = 6$, and $Z = 9$. The secondary decay of such fragments may preserve the enhanced neutron content and lead to emission of final neutron-rich nuclei in the midrapidity direction. However, this explanation may not be obvious for very small species ($Z \lesssim 3$) because

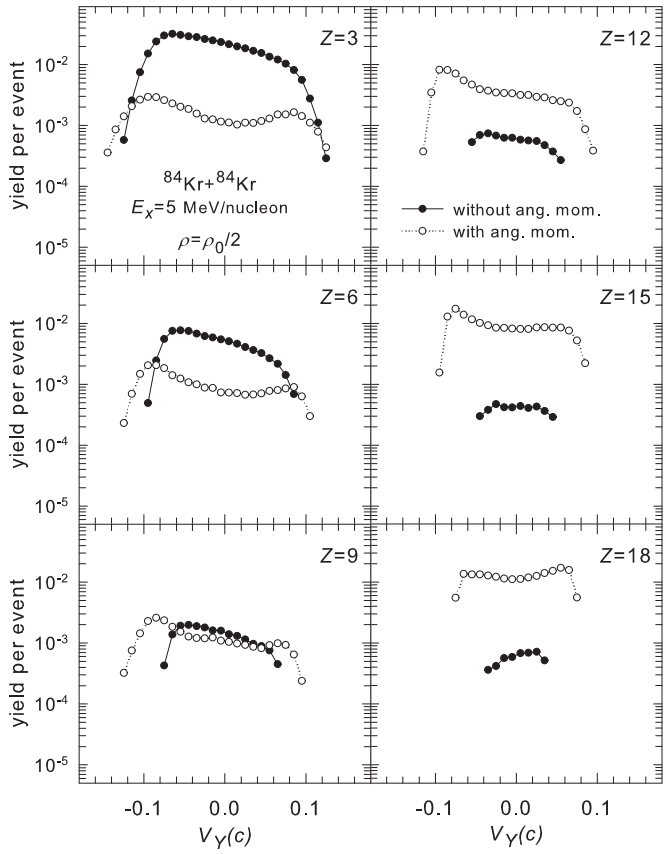

FIG. 5. Relative yields of specific fragments coming from the disintegration of a ^{84}Kr projectile source at the excitation energy of 5 MeV/nucleon as a function of the velocity V_Y in the source frame. Calculations were performed with (open circles; $L = 80\hbar$), and without (filled circles) angular momentum at freeze-out density $\rho = \rho_0/2$.

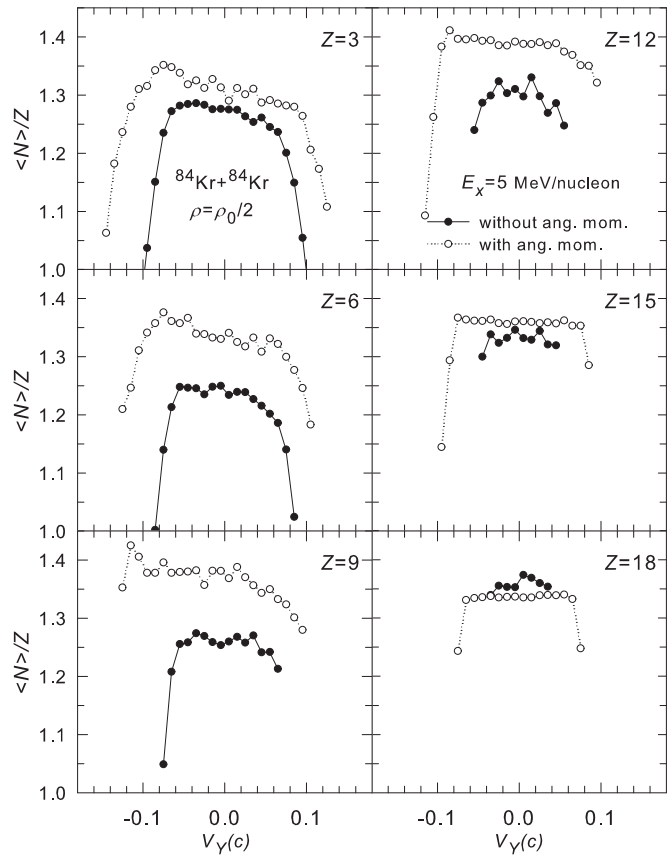

FIG. 6. Mean neutron-to-proton ratios $\langle N\rangle/Z$ as a function of V_Y shown in Fig. 5 (notation is the same).

of their low contribution in partitions with a large angular momentum and because their pre-equilibrium emission is also possible in the reactions. Large species ($Z \gtrsim 15$) lose this sensitivity and they are emitted more uniformly. By including the angular momentum we increase also the velocities of all fragments, and the distributions become broader. The drop in $\langle N\rangle/Z$ at high velocities, actually, for fragments with low yields, is trivially explained by strong Coulomb acceleration if the mass is small.

For completeness, we present how the average charge $\langle Z\rangle$ (top panels) and $\langle N\rangle/Z$ of the fragments with $Z_{\max 1}, Z_{\max 2}$, and $Z_{\max 3}$ change with V_Y in Fig. 7, for cases with and without angular momentum effect. It is in agreement with our previous conclusions on modification of the statistical picture. In particular, one can see a trend of increasing $\langle N\rangle/Z$ towards the midrapidity for $Z_{\max 2}$ and $Z_{\max 3}$ (bottom panels).

C. Dependence of fragment characteristics on distances between sources

It is instructive to investigate how the multifragmentation picture changes with an increasing distance between the sources. This will show the evolution of the decay of the sources towards high-energy collisions. As we know, the decay of an ensemble of isolated statistical sources formed from projectile/target residues describes very good experiments at relativistic collisions [11,15–17]. In our analysis we consider the distances $R_Y = -30$ and $R_Y = -70$ fm. This is consistent with the assumption of multifragmentation times of $\sim$230 and 500 fm/c for the given relative velocity, whereas under the standard multifragmentation time ($\sim$100 fm/c) it corresponds to higher relative velocities between target and projectile sources. The typical separation between the sources in relativistic collisions would be around $\sim$100 fm. We demonstrate how rapidly the whole picture transforms into multifragmentation of isolated sources with the distance.

For this purpose, in Fig. 8, we show the total charge yields and $\langle N\rangle/Z$ of fragments produced at the source density $\rho = \rho_0/2$ for these distances. To clarify the Coulomb contribution, we do not include the angular momentum here. Comparing Fig. 8 with Figs. 1 and 3 one can see that the expected distributions are very close to those obtained in the case of isolated sources, already at $R_Y = -70$ fm. As expected, the decrease in the external Coulomb field leads to enhanced IMF production because of the lower Coulomb barrier. The neutron richness of these fragments increases slightly, and correspondingly, the neutron content of the largest fragment decreases, in correlation with their more uniform distribution in the coordinate space. Similar isospin

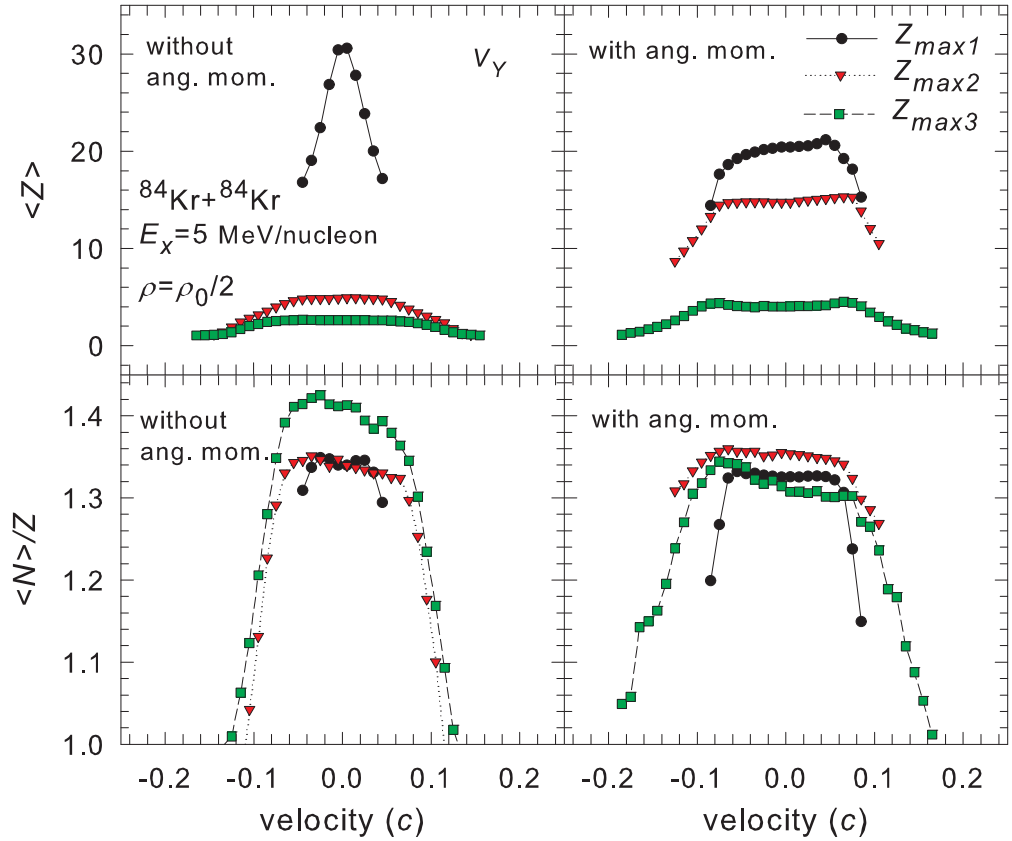

FIG. 7. (Color online) Mean charge Z (top panels) and $\langle N\rangle/Z$ (bottom panels) distributions of the first, second, and third largest hot fragments (Z_{max1}, Z_{max2}, and Z_{max3}) after multifragmentation of a ^{84}Kr projectile source at $E_x = 5$ MeV/nucleon versus V_Y in the source frame. The freeze-out density is $\rho = \rho_0/2$. Left panels represent results without angular momentum; right panels, with angular momentum ($L = 80\hbar$).

distributions in statistical models have been under study for a long time [5,12].

The velocity distributions of the produced $Z = 6$ fragments are shown in Fig. 9. One can see that the predicted anisotropy depends also on the distances between the sources: It decreases with the distance rather smoothly approaching the isotropic distributions, which are naturally expected for the isolated sources. However, a small anisotropy presents even at distances around 30 fm, i.e., the external long-range Coulomb effect can still occur if the fragment formation is relatively rapid.

Some calculations of the collisions with dynamical models predict the formation of a neck-like fragment in the midrapidity region (between the sources). This mechanism is related to the dynamical migration of nucleons and isospin diffusion. For our case, it can be treated as an additional source of the Coulomb field influencing the disintegration of matter in the projectile freeze-out volume. In order to evaluate this effect we have assumed such a neck-like fragment with $A = 12$ and $Z = 6$ consisting of nucleons taken equally from the projectile and the target. In Fig. 10 we show such calculations for the short distance $R_Y = -10.6$ fm and for the formation of IMFs with $Z = 6$. To be more general we have included the angular momentum also. Comparing Fig. 10 with Figs. 5 and 6 we can see again the anisotropy effects related to the external Coulomb influence. In addition, there is a reduction in the total number of IMFs because of the larger Coulomb barrier. Therefore, such a neck-like emission can just enforce the Coulomb influence on the fragment distributions in projectile- and target-like sources.

Another interesting dynamical effect could be the primary modification of the nucleon density profile from the standard uniform one assumed in the statistical sources. It can be considered within the microcanonical approaches, besides the external Coulomb field, e.g., as a spatial modification of the sources [35,36]. It may also lead to special effects, which we plan to investigate in forthcoming works.

To verify our new-found trends we also performed the same calculations for heavier systems, e.g., ^{197}Au + ^{197}Au collisions. In all cases, we got the same qualitative modifications of the standard multifragmentation picture.

IV. RELATION BETWEEN STATISTICAL AND DYNAMICAL DESCRIPTIONS

In this paper we investigate the kinematic characteristics, sizes, and isospin properties of hot fragments within a microcanonical statistical approach. Subsequently, these fragments will be de-excited by emission of light particles, or by the secondary breakup, during their propagation. As shown in many previous works the secondary process can be reliably described within statistical models (see, e.g., Refs. [11] and [17], and references in).

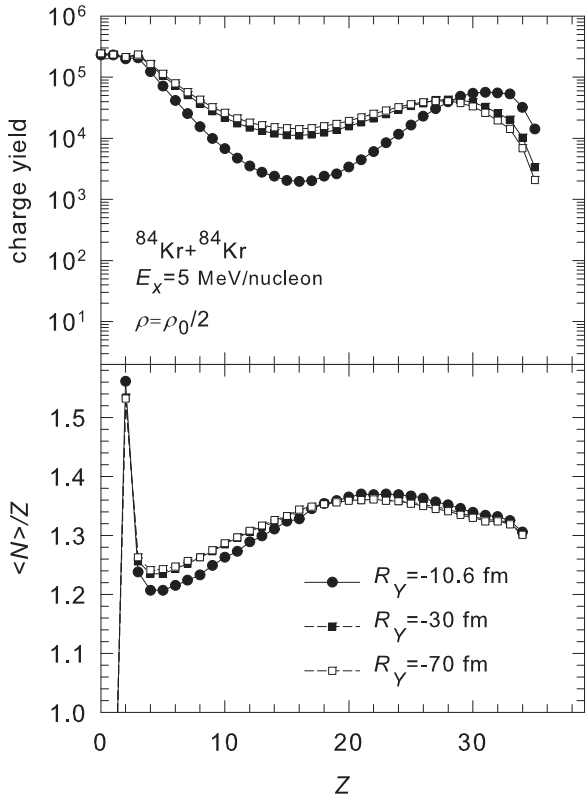

FIG. 8. Total charge yield (top) and mean neutron-to-proton ratios $\langle N\rangle/Z$ (bottom) of all primary fragments produced at freeze-out density $\rho = \rho_0/2$ and at different distances between the sources (see notations in the figure).

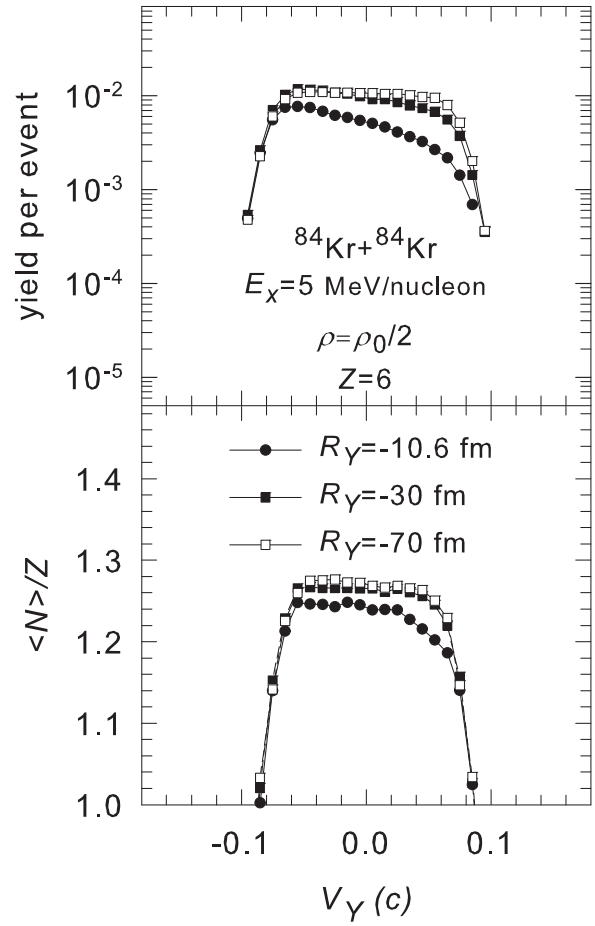

FIG. 9. Yield distribution (top) and mean neutron-to-proton ratios $\langle N\rangle/Z$ (bottom) of primary fragments with $Z = 6$ as a function of their velocity V_Y in the source frame, at different distances between the sources (see notations in the figure). The freeze-out density is $\rho = \rho_0/2$.

It was previously discussed that dynamical models alone may simulate the same evolutionary scenario leading to equilibration and multifragmentation as assumed by statistical models. In other words, is it possible to use only a dynamical description, instead of subdividing the whole reaction into dynamical and statistical stages? Some dynamical approaches try to reach this goal starting from "first principles" like fermionic molecular dynamics [37] and antisymmetrized molecular dynamics [38]. Other approaches, like QMD [39] and BNV [40,41], use semiclassical equations including two-body collisions and some elements of stochasticity. In all cases dynamical simulations are more complicated and time-consuming compared with statistical models. This is why full calculations, e.g., with fermionic and antisymmetrized molecular dynamics models, are usually done for relatively light systems. This prevents using these codes in many cases of nuclear fragmentation, especially when extensive Monte Carlo simulations are required. Another complication is that the mathematical approximations for calculation of the many-body process are usually different at high and low energies, and this requires the involvement of a different kind of model. A natural solution of this problem is to develop hybrid approaches which combine dynamical models for describing the nonequilibrium early stages of the reaction with statistical models for describing the fragmentation of equilibrated sources. In this respect, the statistical and dynamical approaches are complementary and suitable for many practical calculations, which are necessary, e.g., in medicine, space research, and other fields.

One can try dynamical models to describe the fragment (i.e., nucleon cluster) formation at the time of nuclear freeze-out too, as we are doing for hot fragments with statistical models. Actually, it is popular to explain in a dynamical way the formation of neck-like fragments in collisions of heavy ions around the Fermi energy [40]. Also, knowledge of the fragment formation process may be necessary for determination of fragment kinematic characteristics. However, the essential problem in the dynamical approach is the connection to the relatively slow secondary de-excitation stage of the fragment ($\gtrsim 10^2$–10^3 fm/c). This last stage is very important for isotope composition of final cold fragments, which may give access to the symmetry energy of nuclei and nuclear matter. As shown in some dynamical calculations [40], the primary nucleon clusters may have a low density and unusual form. So it is difficult to establish the excitation energy of such clusters [18]. Moreover, a big problem is the evaluation of other properties of these clusters, such as their masses, level densities, and

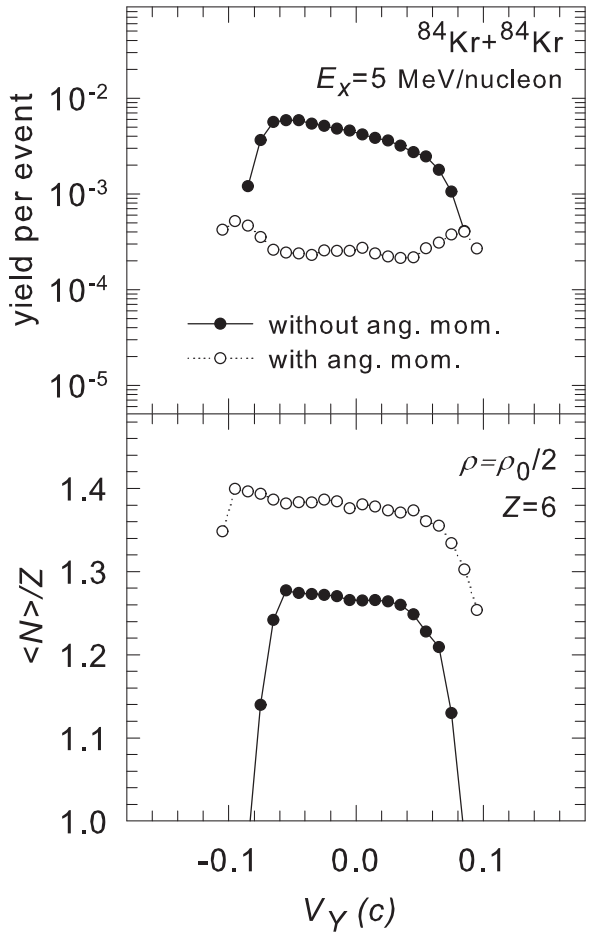

FIG. 10. The same as Fig. 9, however, for the distance $R_Y = -10.6$ fm between the sources and with the presence of the neck-like fragment ($A = 12$, $Z = 6$) at midrapidity between the sources. Calculations without (filled circles) and with (open circles) angular momentum $L = 80\hbar$ are shown.

symmetry energies. The latter are crucial for the subsequent de-excitations leading to cold nuclei. Therefore, the predictions of dynamical models are usually limited to hot fragments. On the contrary, one can easily resolve this problem within the statistical approach. As demonstrated in Refs. [10,12] one can connect the freeze-out properties of hot fragments with their secondary de-excitation and the yield of final isotopes. In this respect, the application of appropriate statistical models to the reactions, which were considered previously only as dynamical processes, opens real chances for involving new data in theoretical analysis. One should bear in mind that the statistical and dynamical approaches are derived from different physical principles. The time-dependent dynamical approaches are based on Hamiltonian dynamics (the principle of minimal action), whereas the statistical models employ the principle of uniform population of the phase space. Actually, these two principles represent complementary methods for describing the physical reality. Therefore, the decision to use statistical or dynamical approaches for the description of nuclear multifragmentation should be made after careful examination of the degrees of equilibration expected in particular cases, and it can only be justified by the comparison with experiment.

In the case of equilibrated sources, the predictions of statistical models are usually in good agreement with experimental data. This is well known in multifragmentation of relativistic projectiles [15,16,42], especially when the chemical equilibrium is established in such reactions, and this equilibrium can be seen in isotopic yields [10,11]. This can also be seen by describing the isospin observables in nucleus-nucleus collisions at lower (Fermi) energies: For example, one can compare dynamical [18] and statistical [19,21,43] analyses of the MSU experimental data. As shown in the present work, the effect of increasing the neutron number in IMFs emitted towards the midrapidity region may also be explained within the statistical picture modified by including the external Coulomb field and angular momentum. Nevertheless, the dynamical models provide other important opportunities by describing nucleon transport and giving information on the nonequilibrium reaction stage. In particular, the pre-equilibrium density and isospin distributions caused by strong interactions can be obtained, as well as the density and isospin gradients. In order to distinguish dynamical and statistical mechanisms one should involve specific experimental characteristics, e.g., isospin and correlations of fragments.

We believe that the most urgent matter in this case is to combine the dynamical and statistical approaches, which can be used correspondingly in the fast and slow stages of the reaction. This would also be in agreement with the previously established physical picture of such reactions and could be verified by available data [44]. For example, there are experimental data demonstrating the trend to increasing neutron richness of IMFs in collisions of nuclei with increasing centrality, i.e., with increasing excitation energy, both in the midrapidity region [45] and in a single equilibrated central source [33]. A dynamical calculation may predict more neutron-rich IMFs in very peripheral collisions since the neutron-rich periphery of nuclei influences the dynamics of IMF formation [40]. Obviously, before comparisons with experiment, these excited IMFs must go through de-excitation. We see two ways to effectively combine the dynamical and statistical approaches: One can use the dynamical density and isospin profile as the input for a statistical approach like the one mentioned in this work. Another way is to take hot fragments after the dynamical calculations and apply de-excitation statistical models which include the modified properties of these fragments [12]. In these cases it would be possible to pursue the full analysis of coming novel experiments aimed predominantly at measuring isotopes in low- and intermediate-energy collisions [26,46].

V. CONCLUSIONS

In conclusion, within the statistical approach we have investigated isotopic characteristics of hot fragments after multifragmention of the Kr-like projectiles in peripheral $^{84}\mathrm{Kr} + {}^{84}\mathrm{Kr}$ collisions around (and possibly higher than) the Fermi energy. It is important and new that we have taken into account Coulomb and angular momentum effects originating after the collision dynamics. We have used the microcanonical

Markov chain approach within the SMM. It is shown that conservation of angular momentum and complicated Coulomb interactions caused by the proximity of target- and projectile-like sources in the freeze-out stage produces significant changes in the multifragmentation picture. New fragment formation trends appear, such as an asymmetry of IMF emission (predominantly towards the midrapidity), increasing the neutron content of these IMFs, correlation (ordering) of the sizes and velocities of fragments, and in-plane emission of large fragments. This is instructive, since in previous years it was assumed that such effects could be explained within dynamical models only. These features may also be preserved after the secondary excitation of hot fragments for the cold fragments, similar to the previously analyzed reactions leading to the production and decay of single isolated sources. Such statistical processes can develop in addition to the special dynamical phenomena, e.g., the neck-like emission. In the future, we plan to apply this new approach to analyze experimental data in intermediate peripheral collisions such as the FAZIA data measured in ^{84}Kr + ^{124,124}Sn reactions at 35 Mev/nucleon [26]. Particular isotopic effects, such as the odd-even staggering of the yield of final fragments studied by the FAZIA Collaboration [46], can also be analyzed within similar statistical approaches. We have also demonstrated the evolution of the multifragmentation picture towards relativistic energy collisions. It is interesting that minor Coulomb effects, in particular, a small anisotropy in the emission of light fragments, may still survive, leading to distortion from the uniform statistical decay, if the disintegration is fast enough.

Some preliminary encouraging results obtained with the suggested approach were already reported [47]. This kind of investigation should show a new connection between dynamical and statistical phenomena in nuclear reactions. We discuss the possibilities for practical and effective combinations of dynamical and statistical approaches. As expected, these reactions may provide us with input to understand the nuclear equation of state and nuclear composition, which are important for determining the properties of nuclear and stellar matter under extreme conditions and their connections to the thermodynamics of stellar matter in astrophysical events [28]. We also believe that our theoretical results may be enlightening for further analysis of the experiments.

ACKNOWLEDGMENTS

We thank G. Casini for stimulating discussions and help with the preparation of the manuscript. This work was supported by TUBITAK (Turkey) under Project No. 113F058. A.S.B. was supported by the GSI Helmholtzzentrum für Schwerionenforschung GmbH and Hessian Initiative for Scientific and Economic Excellence (LOEWE) through the Helmholtz International Center for FAIR.

[1] M. D'Agostino *et al.*, Phys. Lett. B **371**, 175 (1996).
[2] A. S. Botvina, O. V. Lozhkin, and W. Trautmann, Phys. Rev. C **65**, 044610 (2002).
[3] A. S. Botvina and D. H. E. Gross, Nucl. Phys. A **592**, 257 (1995).
[4] D. H. E. Gross, Phys. Rep. **279**, 119 (1997).
[5] A. S. Botvina and I. N. Mishustin, Phys. Rev. C **63**, 061601(R) (2001).
[6] A. S. Botvina, M. Bruno, M. D'Agostino, and D. H. E. Gross, Phys. Rev. C **59**, 3444 (1999).
[7] J. M. Lattimer and M. Prakash, Astrophys. J. **550**, 426 (2001), and references therein.
[8] A. S. Botvina and I. N. Mishustin, Nucl. Phys. A **843**, 98 (2010).
[9] A. Ono, P. Danielewicz, W. A. Friedman, W. G. Lynch, and M. B. Tsang, Phys. Rev. C **68**, 051601(R) (2003).
[10] A. Le Fèvre *et al.*, Phys. Rev. Lett. **94**, 162701 (2005).
[11] R. Ogul, A. S. Botvina, U. Atav, N. Buyukcizmeci, I. N. Mishustin *et al.*, Phys. Rev. C **83**, 024608 (2011).
[12] N. Buyukcizmeci, R. Ogul, and A. S. Botvina, Eur. Phys. J. A **25**, 57 (2005).
[13] A. S. Botvina, N. Buyukcizmeci, M. Erdogan, J. Łukasik, I. N. Mishustin, R. Ogul, and W. Trautmann, Phys. Rev. C **74**, 044609 (2006).
[14] A. S. Botvina and I. N. Mishustin, Phys. Lett. B **294**, 23 (1992).
[15] A. S. Botvina *et al.*, Nucl. Phys. A **584**, 737 (1995).
[16] H. Xi *et al.*, Z. Phys. A **359**, 397 (1997).
[17] J. P. Bondorf *et al.*, Phys. Rep. **257**, 133 (1995).
[18] T. X. Liu *et al.*, Phys. Rev. C **69**, 014603 (2004).
[19] R. Ogul *et al.*, J. Phys. G: Nucl. Part. Phys. **36**, 115106 (2009).
[20] N. Buyukcizmeci *et al.*, Acta Phys. Pol. B **42**, 697 (2011).
[21] N. Buyukcizmeci *et al.*, J. Phys. G: Nucl. Part. Phys. **39**, 115102 (2012).
[22] J. Iglio *et al.*, Phys. Rev. C **74**, 024605 (2006).
[23] G. A. Souliotis, A. S. Botvina, D. V. Shetty, A. L. Keksis, M. Jandel, M. Veselsky, and S. J. Yennello, Phys. Rev. C **75**, 011601(R) (2007).
[24] A. S. Botvina, arXiV:nucl-th/0008068.
[25] M. Jandel, A. S. Botvina *et al.*, J. Phys. G: Nucl. Part. Phys. **31**, 29 (2005).
[26] S. Barlini *et al.*, Phys. Rev. C **87**, 054607 (2013).
[27] S. Das Gupta and A. Z. Mekjian, Phys. Rev. C **57**, 1361 (1998).
[28] N. Buyukcizmeci *et al.*, Nucl. Phys. A **907**, 13 (2013).
[29] A. S. Botvina, A. S. Iljinov, and I. N. Mishustin, Sov. J. Nucl. Phys. **42**, 712 (1985).
[30] A. S. Botvina *et al.*, Nucl. Phys. A **475**, 663 (1987).
[31] S. Fritz *et al.*, Phys. Lett. B **461**, 315 (1999).
[32] V. E. Viola, K. Kwiatkowski, J. B. Natowitz, and S. J. Yennello, Phys. Rev. Lett. **93**, 132701 (2004).
[33] P. Milazzo *et al.*, Phys. Rev. C **62**, 041602 (2000).
[34] J. Colin *et al.*, Phys. Rev. C **67**, 064603 (2003).
[35] J. Lukasik *et al.*, AIP Conf. Proc. **610**, 711 (2002).
[36] A. Le Fevre *et al.*, Nucl. Phys. A **735**, 219 (2004).
[37] H. Feldmeier, Nucl. Phys. A **681**, 398c (2001).
[38] A. Ono and H. Horiuchi, Phys. Rev. C **53**, 2958 (1996).
[39] W. Bauer *et al.*, Annu. Rev. Nucl. Part. Sci. **42**, 77 (1992); B. A. Li, Phys. Rev. C **47**, 693 (1993); J. Konopka *et al.*, Progr. Part. Nucl. Phys **30**, 301 (1993); M. Colonna *et al.*, Nucl. Phys. A **589**, 160 (1995); C. Fuchs and H. Wolter, *ibid.* **589**, 732 (1995); A. S. Botvina *et al.*, Phys. At. Nucl. **58**, 1703 (1995).
[40] V. Baran *et al.*, Nucl. Phys. A **703**, 603 (2002).
[41] P. Napolitani, M. Colonna, F. Gulminelli, E. Galichet, S. Piantelli, G. Verde, and E. Vient, Phys. Rev. C **81**, 044619 (2010).

[42] R. P. Scharenberg *et al.*, Phys. Rev. C **64**, 054602 (2001).
[43] C. B. Das *et al.*, Phys. Rep. **406**, 1 (2005).
[44] Ph. Chomaz, F. Gulminelli, W. Trautmann, and S. J. Yennello (eds.), *Dynamics and Thermodynamics with Nuclear Degrees of Freedom* (Springer, Berlin, 2006); Eur. Phys. J. A **30**, 1 (2006).
[45] H. Xu *et al.*, Phys. Rev. C **65**, 061602 (2002).
[46] S. Piantelli *et al.*, Phys. Rev. C **88**, 064607 (2013).
[47] A. Ergun *et al.*, International Conference on Nuclear Fragmentation NUFRA2013, Kemer, Turkey, 29 September–6 October (2013), http://fias.uni-frankfurt.de/historical/nufra2013.